Modeling the Statistics of Elementary Calcium Release Events

Ghanim Ullah and Peter Jung
Department of Physics and Astronomy and Quantitative Biology Institute, Ohio University, Athens, Ohio

ABSTRACT Elementary Ca^{2+} signals, such as "Ca^{2+} puffs", which arise from the release of Ca^{2+} from endoplasmic reticulum through small clusters of inositol 1,4,5-trisphosphate receptors, are the building blocks for intracellular Ca^{2+} signaling. The small number of release channels involved during a Ca^{2+} puff renders the puffs stochastic, with distributed amplitudes, durations, and frequency, well characterized experimentally. We present a stochastic model that accurately describes simultaneously the statistical properties of the duration, amplitudes, frequencies, and spatial spread with a single set of parameters.

INTRODUCTION

Ca^{2+} signaling is one of the most important intracellular signaling mechanisms, controlling, e.g., the contraction of muscle cells, the release of neurotransmitter from neurons and astrocytes, and metabolic processes in liver and pancreas. Calcium signaling is characterized by a hierarchy of processes ranging from the spatially and temporally limited Ca^{2+} puffs over global oscillations (in small cells, such as astrocytes) to propagating waves in large cells like oocytes (1–4).

The amplitude, duration, and spatial spread of elementary calcium release events (puffs and blips) varies widely (2,5,6). Sun et al. (5) showed that the amplitude of single events has a skewed distribution with a maximum F/F_0 (ratio of the fluorescence at each pixel during a response to the resting fluorescence at that pixel before simulation of Oregon Green 488 BAPTA-1) at 1.5 and a tail as high as 3.5. The signal mass distribution of discrete events is exponential (Fig. 8 *B* of Sun et al. (5)). The smallest events resolved correspond to a signal mass of 2×10^{-20} mole and large events to 2×10^{-18} mole. A current underlying a large puff is estimated by this study at 2.5 pA. This current was used to estimate the number of open channels involved in a single puff at five to eight. Another independent study led to a distribution where amplitudes span a range of values from a few tens to several hundreds of nanomolars (6).

Event-duration distribution (full duration at half-maximal amplitude (FDHM)) shows a peak at ~150 ms and an exponential decay for durations up to 600 ms (5,6). The distribution for spatial spread (full width at half magnitude (FWHM)) of puffs, obtained by Haak et al. (7), ranges from 0.5 μm to 3.5 μm (Fig. 5 *B* of Haak et al. (7)). The time interval between consecutive puffs follows a distribution with a peak at ~1.5 s or 3.4 s, depending on whether the puffs are focal (puffs that initiated Ca^{2+} waves) or nonfocal (puffs that could not initiate Ca^{2+} waves) (1).

A central role for the diverse intracellular Ca^{2+} patterns is played by the release of Ca^{2+} from the endoplasmic reticulum (ER) through small clusters of release channels called inositol 1,4,5-trisphosphate receptors (IP_3Rs) (see Falcke (8) for an excellent review), which have an estimated 10–40 channels per cluster (9–11). Various studies on the structure of IP_3Rs revealed a flower-like structure fitting within a cube with sides of ~18 nm (12). Thus, 10–40 IP_3Rs would correspond to a cluster of the order of 50—150 nm in size. These clusters are randomly distributed, with an average distance of ~2–3 μm (11,13). The small number of channels per cluster causes a stochastic release of Ca^{2+} through the cluster. The collective opening and closing of several channels in a single cluster causes the wide distribution of event sizes described above.

A mathematical description of Ca^{2+} puffs should reproduce the statistical properties of Ca^{2+} puffs, i.e., the distribution of puff amplitudes, puff durations, and frequencies. The available detailed statistical features of puffs are indeed an excellent test bench for mathematical models of calcium signaling. Stochastic versions of older models, like the DeYoung-Keizer model (14) or derivatives such as the Li-Rinzel model (15), can explain a number of features like the puff amplitude distribution (10), but predict event durations on the order of seconds. On the other hand, the peak of experimentally obtained distribution of duration is of the order of 150 ms (5,6) (also see Fig. 1). Similar problems are encountered in Swillens et al. (11) for realistic IP_3 concentrations used in experiments that investigate calcium puffs through uncaging of IP_3 (see Results).

In this article, we investigate whether a stochastic version of the kinetic model of the IP_3Rs by Sneyd and Dufour (16) (SD model) can be used to accurately describe the experimentally observed statistical properties of Ca^{2+} puffs, such as distributions of puff duration, puff amplitude, frequency, and spatial extent. The SD model incorporates new insights into the kinetics of the IP_3 receptor, including non-mass-action law kinetics for Ca^{2+} binding and serial binding of IP_3 and Ca^{2+} to activating binding sites. However, the SD

Submitted August 29, 2005, and accepted for publication February 7, 2006.

Address reprint requests to Ghanim Ullah, Dept. of Physics and Astronomy, Ohio University, Athens, OH 45701. Tel.: 740-593-9671; Fax: 740-593-0433; E-mail: ghanimul@helios.phy.ohiou.edu.

0006-3495/06/05/3485/11 $2.00

doi: 10.1529/biophysj.105.073460

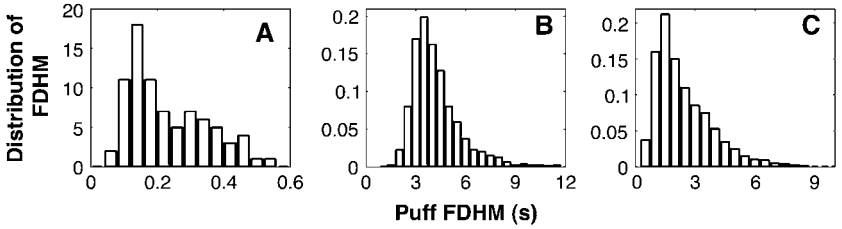

FIGURE 1 The distribution of puff durations observed by Sun et al. (5) (*A*) is compared with predictions using stochastic versions (10) of the Li-Rinzel model (15) (*B*) and the DeYoung-Keizer model (14) (*C*).

model, is modified to resolve an ambiguity in the kinetic states following Falcke (8).

A cluster is defined by a small group of IP_3Rs that are geometrically close enough that, on the timescale of the channel kinetics, they share the same Ca^{2+} concentration released by the channels. We model a single cluster of IP_3R channels embedded in the ER membrane in contact with the cytosole, allowing the Ca^{2+} released by ER to diffuse. Based on the estimates of Swillens et al. (11) and Shuai et al. (13), we consider the cluster to be composed of 20 IP_3Rs. We study the statistical distribution of amplitude, spatial spread, lifetime, and interpuff intervals and compare with the experimental data.

MATERIALS AND METHODS

The IP_3R model

On the typical timescale of calcium release events (≈100 ms) and using the effective Ca^{2+} diffusion coefficient of 30.0 $\mu m^2\ s^{-1}$, the diffusion length is of the order of $\sqrt{30\times0.1}\mu m \approx 1.73\mu m$, and thus larger than the size of the cluster. Thus, even in the absence of direct physical interaction, the IP_3Rs within one cluster effectively interact by being exposed to almost the same Ca^{2+} concentration. This interaction gives rise to the collective events underlying the calcium puffs described above.

For a single IP_3 receptor we adopted the kinetic model put forward by Sneyd and Dufour (16), according to which the receptor is composed of four independent subunits, each with four binding sites, one for IP_3, two for Ca^{2+} activation, and one for Ca^{2+} inactivation. The full kinetic scheme of a subunit is shown in Fig. 2 *A*. Lumping all the R states (R′, $\overline{R}$, and $\tilde{R}$) under R, $\tilde{O}$ and $\overline{O}$ states under O, and $\tilde{A}$ and $\overline{A}$ states under A, the subunit has essentially six states R, O, A, S, I_1, and I_2 (Fig. 2 *B*). In state R, neither Ca^{2+} nor IP_3 is bound. The subunit can inactivate directly from this state, i.e., going to state I_1, by binding Ca^{2+}. Before the subunit can switch into the activated state A, it has to bind first IP_3 (state O) and subsequently Ca^{2+}. In the activated state, the subunit can inactivate directly by binding Ca^{2+} to the inactivating binding site. While in the open state, O, the subunit can switch spontaneously to the shut state S if IP_3 is bound. Based on this skeleton of the model, the triangular motifs, e.g., $\tilde{R}$, R′, and I_1, were introduced to generate transition rates between R (lumped) and I_1 that do saturate with increasing Ca^{2+} concentration (for details see Falcke (8) and Sneyd and Dufour (16)). The downside of this method, however, is that these motifs are not conservative with respect to Ca^{2+}. For example, if a subunit were to go through the cycle $\tilde{A}\rightarrow\overline{A}\rightarrow I_2\rightarrow\tilde{A}$, it would pick up a Ca^{2+} ion (at the activating site) with each transition from $\tilde{A}$ to $\overline{A}$ without losing it in another transition of the cycle. The motifs consisting of $\tilde{R}$, $\overline{R}$, and $\tilde{O}$ and $\acute{R}$, $\tilde{R}$, and I_1 have the same problem. To solve this problem, we followed Falcke (8) and introduced three additional states $\acute{O}$, $\bar{I}_1$, and $\bar{I}_2$ into the scheme of Fig. 2 *A*. Thus, we replaced the motifs ($\acute{R}$, $\tilde{R}$, I_1), ($\tilde{R}$, $\overline{R}$, $\tilde{O}$), and ($\tilde{A}$, $\overline{A}$, I_2) of Fig. 2 *A* with new motifs shown in Fig. 2 *C* (the states I_1 and I_2 of Fig. 2 *A* are represented by $\tilde{I}_1$ and $\tilde{I}_2$ in Fig. 2 *C*). For the channel to be open, all four subunits must be activated.

Consistency with the original Sneyd-Dufur model

Since the basic structure of our model is taken from the model by Sneyd and Dufour (16), we needed to verify that the modifications we made did not interfere with its ability to describe Ca^{2+} oscillations. To compare our prediction with that of the original Sneyd-Dufour model (16), we followed their protocol in simplifying the equations through adiabatic elimination. In the scheme of Fig. 2, *A* and *C*, the following transitions are fast and the associated states can be considered in instantaneous equilibrium: $\tilde{R}\rightleftharpoons\overline{R}$, $\tilde{R}\rightleftharpoons\acute{R}$, $\tilde{O}\rightleftharpoons\acute{O}$, $\tilde{O}\rightleftharpoons\overline{O}$, $\tilde{I}_1\rightleftharpoons\bar{I}_1$, $\tilde{A}\rightleftharpoons\acute{A}$, and $\tilde{I}_2\rightleftharpoons\bar{I}_2$. We thus obtain $c\tilde{R}=L_1\acute{R}$, $c\tilde{R}=L_3\overline{R}$, $c\tilde{O}=L_5\overline{O}$, $c\tilde{O}=L_3\acute{O}$, $c\tilde{I}_1=L_1\bar{I}_1$, $c\tilde{A}=L_1\overline{A}$, and $c\tilde{I}_2=L_1\bar{I}_2$. Now, defining $R=\overline{R}+\tilde{R}+\acute{R}$, $O=\overline{O}+\tilde{O}+\acute{O}$, $I_1=\bar{I}_1+\tilde{I}_1$, $A=\tilde{A}+\overline{A}$, and $I_2=\tilde{I}_2+\bar{I}_2$, we arrive at the simplified kinetic scheme for the subunits of the IP_3 receptors shown in Fig. 2 *B*:

$$\begin{aligned}
\frac{dR}{dt} &= \phi_{-2}O - \phi_2 pR + (k_{-1}+l_{-2})I_1 - \phi_1 R\\
\frac{dO}{dt} &= \phi_2 pR - (\phi_{-2}+\phi_4+\phi_3)O + \phi_{-4}A + k_{-3}S\\
\frac{dA}{dt} &= \phi_4 O - (\phi_{-4}+\phi_5)A + (k_{-1}+l_{-2})I_2\\
\frac{dI_1}{dt} &= \phi_1 R - (k_{-1}+l_{-2})I_1\\
\frac{dI_2}{dt} &= \phi_5 A - (k_{-1}+l_{-2})I_2,
\end{aligned} \tag{1}$$

with the saturating (non-mass-action) binding rates

$$\begin{aligned}
\phi_1 &= \frac{(k_5 c + L_1 k_1)c}{L_1 + c\left(1+\frac{L_1}{L_3}\right)}\\
\phi_2 &= \frac{l_4 c + L_3 k_2}{L_3 + c\left(1+\frac{L_3}{L_1}\right)}\\
\phi_{-2} &= \frac{(l_{-4}+k_{-2})(c+L_3)}{L_3 + c\left(1+\frac{L_3}{L_5}\right)}\\
\phi_3 &= \frac{L_5 k_3}{L_5 + c\left(1+\frac{L_5}{L_3}\right)}\\
\phi_4 &= \frac{(k_4 L_5 + l_6)c}{L_5 + c\left(1+\frac{L_5}{L_3}\right)}\\
\phi_{-4} &= \frac{k_{-4}+l_{-6}}{1+\frac{c}{L_1}}\\
\phi_5 &= \frac{(k_5 c + L_1 k_1)c}{L_1 + c}.
\end{aligned} \tag{2}$$

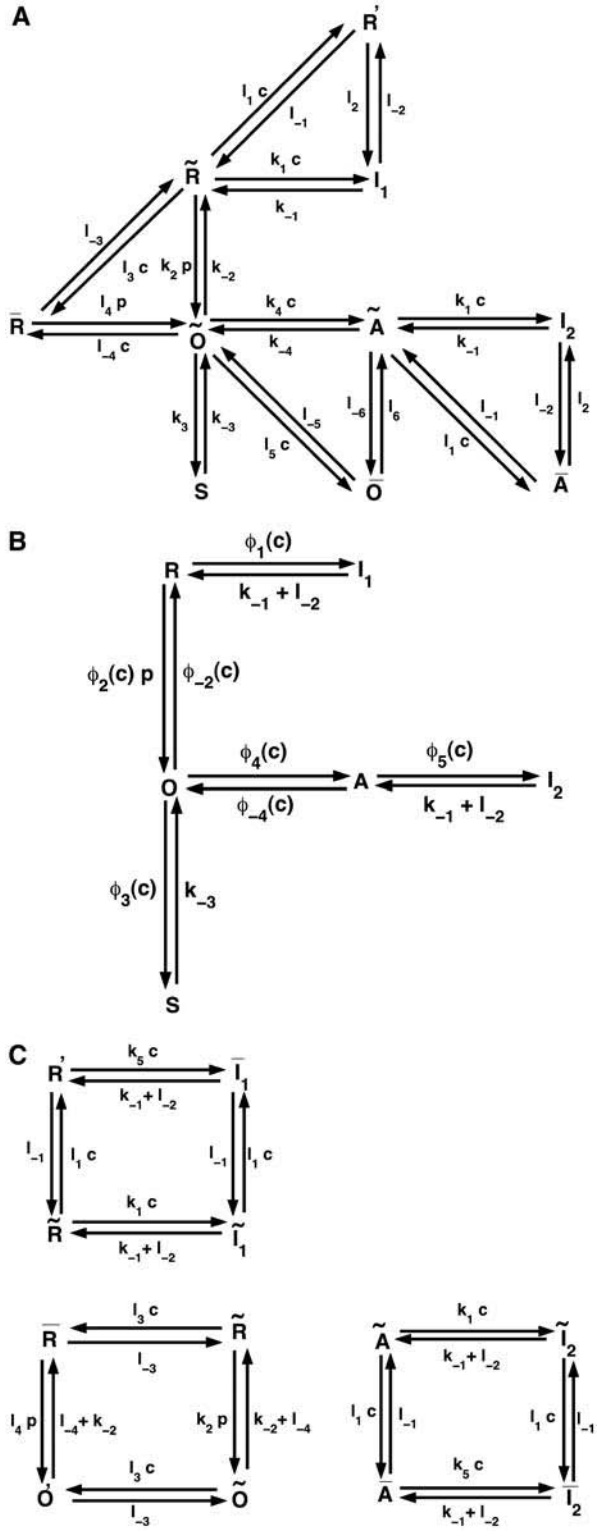

FIGURE 2 (*A*) The full model for one subunit of the IP_3R: *R*, receptor; *O*, open state; *A*, activated state; *S*, shut state; *I*, inactivated state. *c*, Ca^{2+} concentration; *p*, IP_3 concentration (16). (*B*) Simplified scheme of the model with lumped nodes. Considering the fast equilibrium, this scheme is equivalent to the scheme of *A*. The open probability of the receptor for this scheme is $(0.1O + 0.9A)^4$, i.e., (N_0/N) in Eq. 1 is replaced by $(0.1O + 0.9A)^4$. (*C*) Modifications of the triangular motifs of the SD model ($\acute{R}$, $\tilde{R}$, I_1), ($\vec{R}$, $\bar{R}$, $\tilde{O}$), and ($\tilde{A}$, $\bar{A}$, I_2) in *A* by rectangular motifs.

The steady-state open probability of the model (Eqs.1 and 2) as a function of the cytosolic Ca^{2+} concentration for various IP_3 concentrations exhibits a bell-shaped curve for physiologically relevant IP_3 concentrations (results not shown). In Fig. 3, we show the bifurcation diagram of this reduced model with the IP_3 concentration as the control parameter. There is one steady state for low IP_3 concentrations, which loses stability at $IP_3 = 5.34\ \mu M$. This state remains unstable for $IP_3 < 11.73\ \mu M$, above which it gains stability through a subcritical Hopf bifurcation and remains stable as the IP_3 concentration increases further.

To compare our simplified scheme to that of the SD model (17), we consider the bifurcation diagram of the reduced scheme with c_t as the control parameter (results not shown). The bifurcation diagram from our model is very similar to Fig. 2 (plot for a closed-cell model) of (17). However, the range of c_t values where the model shows oscillatory behavior is slightly different. Thus, despite the change of the motifs, the model remains effectively similar to the original model (16).

Spatiotemporal cytosolic Ca^{2+} dynamics

As Ca^{2+} is released through the cluster of IP_3Rs, it can spread out in the cytosol by diffusion. The spread of released Ca^{2+} affects the dynamics of the subunits, as it lowers the Ca^{2+} concentration at the channel cluster and thus plays an important role for the time course of the release event. The spread is modulated by mobile and stationary buffers that absorb free Ca^{2+} and/or diffuse bound calcium. The experimental study of Dargan et al. (18) showed that EGTA (a buffer with a small ''on rate'') disrupts cluster-cluster interactions, thus dissociating Ca^{2+} waves into local signals. BAPTA (a fast buffer), on the other hand, promotes the ''globalization'' of Ca^{2+} signals. Such processes have been modeled with a myriad of reaction-diffusion equations for each buffer (19). As we only consider single puffs and their statistical properties, and not the interaction of clusters, we model the spread of released Ca^{2+} by diffusion with an effective diffusion constant (20). Experimentally derived values of effective diffusion coefficients from confocal line scans (21) are $\sim 30\ \mu m^2/s$.

Thus, the spatiotemporal dynamics of the cytosolic Ca^{2+} concentration, *c*, is modeled by a reaction diffusion equation with a stochastic term describing the influx of Ca^{2+} through the IP_3Rs. If we define $V_{cluster}$ as the maximum flux of Ca^{2+} generated by the channel cluster, the source density for cytosolic calcium is given by

$$J_{IPR} = V_{cluster}\left(\frac{N_o}{N}\right)(c_e - c), \tag{3}$$

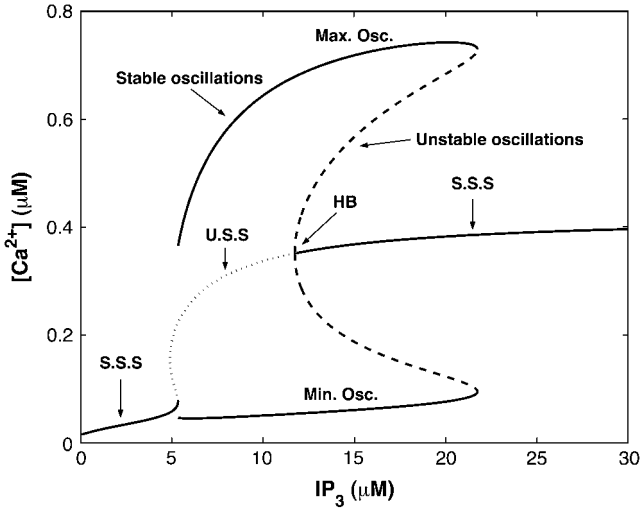

FIGURE 3 Bifurcation diagram of the simplified model, where S.S.S indicates stable steady states and U.S.S. unstable steady states; $V_{cluster} = 0.96\ s^{-1}$.

where c_e denotes the calcium concentration in the ER, N_o the number of open channels, and N the total number of channels in the cluster. It is assumed that the spatial variability of the flux across the area of the channel cluster can be neglected. The leakage of Ca^{2+} from ER to cytoplasm is described by

$$J_{leak} = V_{leak}(c_e - c). \quad (4)$$

Following Sneyd et al. (17), we used conservation of Ca^{2+} to eliminate the Ca^{2+} concentration in the ER, c_e, by $c_e = \gamma(c_t - c)$, with c_t the total calcium concentration inside the cell, c the average cytosolic Ca^{2+} concentration, and γ the ratio of cytoplasmic volume to ER volume.

Calcium is removed from the cytoplasm by the ATP-dependent sarcoendoplasmic reticulum Ca^{2+} pump. We assumed that these pumps are distributed uniformly on the ER membrane and that the pump-flux is described by the quasi-Hill formula

$$J_{pump} = \left(\frac{V_{pump}c}{K_p + c}\right)\left(\frac{1}{c_e}\right), \quad (5)$$

where negative feedback from the luminal calcium concentration is taken into account through the term $1/c_e$. This term avoids overloading the ER with calcium by reducing the pump flow if luminal calcium is high. Denoting the effective diffusion coefficient of Ca^{2+} by D, the equation for the cytosolic calcium concentration has the form

$$\frac{dc}{dt} = D\nabla^2 c + \zeta(x,y) \times J_{IPR} + J_{leak} - J_{pump}, \quad (6)$$

where the form function $\zeta(x,y)$ is 1 at a cluster location and 0 otherwise. The effective diffusion coefficient D incorporates the effect of buffers. We use values for the effective diffusion coefficient derived from confocal line scans (21) of $\sim 30 \mu m^2/s$. Our model describes an isolated cell where the total amount of Ca^{2+} is conserved. Only the exchange of Ca^{2+} between cytoplasm and ER is taken into account. Table 1 lists the values of all model parameters.

TABLE 1 Model parameters

Parameter	Value
Cluster flux coefficient $V_{cluster}$	600–800 s^{-1}
Leak flux coefficient V_{Leak}	0.002 s^{-1}
Maximum Ca^{2+} uptake V_{Pump}	120 μM^2 s^{-1}
Pump dissociation coefficeint K_p	0.18 μM
Diffusion coefficient of free Ca^{2+} D	25-35 μm^2 s^{-1}
Total Ca^{2+} concentration inside the cell c_t	13.0 μM
Cytoplasm volume/ER volume (γ)	5.405
Channel subunit parameters ($L_i = l_{-i}/l_i$)	
k_1	0.64 μM^{-1} s^{-1}
k_{-1}	0.04 s^{-1}
k_2	37.4 μM^{-1} s^{-1}
k_{-2}	1.4 s^{-1}
k_3	0.11 s^{-1}
k_{-3}	29.8 s^{-1}
k_4	4.0 μM^{-1} s^{-1}
k_{-4}	0.54 s^{-1}
k_5	2.0 μM^{-1} s^{-1}
l_1	10.0 μM^{-1} s^{-1}
l_3	100.0 μM^{-1} s^{-1}
l_5	0.1 μM^{-1} s^{-1}
L_1	0.12 μM
L_3	0.025 μM
L_5	38.2 μM
l_2	1.7 s^{-1}
l_{-2}	0.8 s^{-1}
l_4	1.7 μM^{-1} s^{-1}
l_{-4}	2.5 s^{-1}
l_6	4707.0 s^{-1}
l_{-6}	11.4 s^{-1}

Stochastic simulation of the Ca^{2+} release through a cluster of channels

Each subunit of an IP_3R undergoes stochastic transitions between its states through stochastic binding and dissociation of the agonist. Thus, the state of the channel will be subject to stochastic fluctuations. If the number of channels per cluster is large, these fluctuations average out under the assumption that Ca^{2+} assumes a uniform steady state across the cluster on the timescale of the channel kinetics. The small number of release channels per cluster requires stochastic modeling of the channels and subunits (9,10,19,22). Since the cluster is small, and thus the number of subunits is small, we can afford to simulate each subunit and each transition directly. If the subunit is at time t in a state i, we have to determine the probabilities with which it remains in that state or switches into another state allowed by the kinetic scheme in Fig. 2 within the time interval δt. For example, if a subunit is in state $\tilde{R}$, possible transitions are to states $\acute{R}$, $\tilde{I}_1$, $\tilde{O}$, and $\overline{R}$. For a sufficiently small time interval δt, the probabilities for these transitions are given by

$$\begin{aligned} P_1 &\equiv P_{(\tilde{R}\to\acute{R})} = l_1 c\delta t, \\ P_2 &\equiv P_{(\tilde{R}\to\tilde{I}_1)} = k_1 c\delta t, \\ P_3 &\equiv P_{(\tilde{R}\to\overline{R})} = l_3 c\delta t, \\ P_4 &\equiv P_{(\tilde{R}\to\tilde{O})} = k_2 p\delta t, \end{aligned} \quad (7)$$

for which the values of the rates are listed in Table 1 and the Ca^{2+} concentration referred to in these rates is the calcium at the channel cluster. The probability for the subunit to remain in its initial state $\tilde{R}$ is given by $P_5 \equiv P_{(\tilde{R}\to\tilde{R})} = 1 - (P_1 + P_2 + P_3 + P_4)$. To determine a transition, we followed the procedure outlined in part by the Gillespie algorithm (23). The unit interval is divided into five subintervals of lengths $P_i\delta t$, each subinterval i representing the probability for one of the possible transitions. If a random number α, drawn from a uniform distribution over the unit interval, falls into the subinterval $P_i\delta t$, the corresponding transition is performed. This procedure was followed for each subunit at each time interval δt. The time interval δt was kept sufficiently small for the linear dependence of P_i on the time interval to remain valid. The probability for the subunit to remain in the same state after δt was always >95%. For most of the simulations in this study, a time step of 2×10^{-5} s was used.

To incorporate the cytosolic diffusion of Ca^{2+}, we considered a planar patch of the ER membrane of size 5 $\mu m \times 5$ μm. The patch was discretized and represented by a two-dimensional lattice with grid distance Δx. The Ca^{2+} concentration thus only depended on the coordinates (x,y) of the flat ER membrane. A single cluster of 20 IP_3Rs was placed at the center of the patch as a point source of Ca^{2+}, regardless of its actual physical size. It can be easily shown in a one-dimensional diffusion equation with a distributed source density that such a procedure generates an accurate Ca^{2+} profile outside the channel cluster. Such a procedure is standard in classical mechanics and electrodynamics, where distributions of masses and charges are represented by point masses and point charges. We solved the partial differential equations by a forward difference method (24), with a spatial discretization of $\Delta x = 50$ nm. We considered the boundary conditions where calcium can diffuse out of the integrating patch to avoid piling up of Ca^{2+} but cannot enter the patch from outside. We successfully tested the validity of the point-source release approximation at the cluster site by using a finer grid (of 20 nm) and distributing the channels over several grid elements with independent stochastic simulations of the Ca^{2+} release within those grid elements. Differences between the results presented here were extremely small.

RESULTS

The stochastic scheme described above allowed us to simulate calcium puffs generated by a single cluster. The simulation was performed for a cluster of 20 IP_3Rs placed in a 5 μm $\times$ 5 μm cytosolic region with an effective Ca^{2+} diffusion coefficient of 30 $\mu m^2\ s^{-1}$ and IP_3 concentration of 5.0 μM (for a discussion of this value, see section Amplitude distribution of Ca^{2+} puffs). To be consistent with the experimental analysis of puffs, the Ca^{2+} concentration was averaged across an area of 1 μm^2 that includes the cluster of IP_3Rs. In Fig. 4 *A*, we show a representative example of the time course of a Ca^{2+} puff compared with the time course generated with a stochastic De Young-Keizer model (14) (Fig. 4 *B*) and an experimentally observed puff (Fig. 4 *D*). Each of the spikes in Fig. 4 *A* represents a Ca^{2+} puff.

By visual comparison we can conclude that our new stochastic model generates puffs on a timescale consistent with experimental data. In the following sections, we generate statistical measures of the puffs, such as amplitude distribution and width distribution, to compare the model predictions with experimental data in more detail.

Fig. 4 *C* shows the total number of open channels corresponding to the time course of the Ca^{2+} concentration shown in Fig. 4 *A*. The stochastic opening of channels initiates stochastic Ca^{2+} release events. The resulting elevated Ca^{2+} concentration in turn causes the termination of puffs. From our simulations, the number of open channels for the larger events (puffs) is four to ten, which is close to the five to eight estimated in Parker's lab (5) from their confocal line-scan data.

In Fig. 4 *E*, we show the temporal evolution of a single puff obtained from simulations in Fig. 4 *A* and compare it with the experimental puffs (Fig. 4 *D*) (5); the timescale of theoretical puffs and experimental puffs agrees well. Puffs

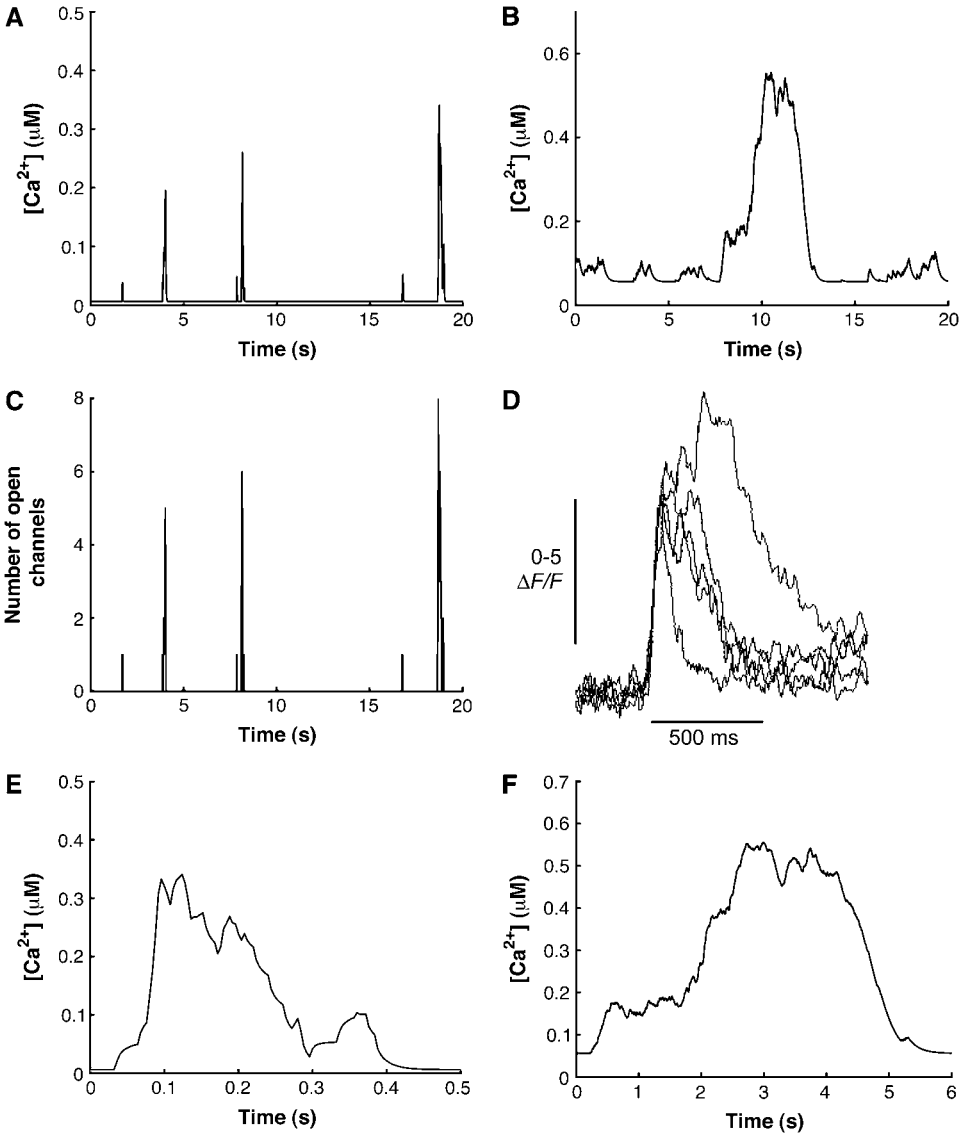

FIGURE 4 Calcium puffs of a cluster of 20 IP_3Rs (IP_3 = 5.0 μM, $V_{cluster}$ = 600.0 s^{-1}, and D = 30.0 $m^2\ s^{-1}$) predicted by our model (*A*) are compared with those generated by the stochastic De Young-Keizer model (*B*) and experiment (*D*). (*C*) Number of open channels during each release event. (*D*) Information taken from experimental data in Sun et al. (5). (*E*) Temporal evolution of a single puff from simulations in panel *A*. (*F*) Temporal evolution of a single puff obtained from a stochastic version of the De Young-Keizer model (14).

obtained from the stochastic version of the De Young-Keizer model (14) (Fig. 4 *F*) are much longer than the experimental puffs.

The Ca^{2+} concentration around a single cluster with open channels is strongly localized, as shown in Fig. 5. Since the system is isotropic, the Ca^{2+} profiles are radially symmetric and can be characterized by cross sections. Such a cross section is shown in Fig. 5. In this case, the Ca^2 concentration decayed by 82% at a distance 0.82 μm from the center of the cluster, which gives a decay constant equal to 0.24 μm^{-1}. The decay constant is obtained by fitting the Ca^{2+} concentration profile in Fig. 5 to the exponential curve. Note that the actual profile is not as sharp as Fig. 5 indicates, since the point-source method produces profiles that are not accurate within the cluster. Within the cluster, the profile is relatively flat, with an almost constant Ca^{2+} concentration (see Appendix).

Amplitude distributions of Ca^{2+} puffs

As shown in Fig. 4 *C*, the number of open channels during a single puff varies stochastically. As a consequence, the amplitudes of Ca^{2+} puffs span a considerable range of values. Calcium puffs are generated experimentally by uncaging IP_3 or a homolog of IP_3 into the cell. IP_3 is released with an ultraviolet laser flash, but the exact amount is not known and there is uncertainty about the cytosolic concentrations of IP_3 required to evoke Ca^{2+} signals among different cells (see, for example, Bird et al. (25) and Leybaert et al. (26)). We simulated the IP_3R clusters for a range of IP_3 concentrations between 4.0 μM and 10 μM. However, the exact value of the IP_3 concentration does not affect the main findings of our study, because the affinity of IP_3Rs can be adjusted as necessary to match the properties of different cells. For example, for smaller IP_3 concentrations, increasing the IP_3 binding rates l_4 and k_2 (see Fig. 2) yields statistical properties of puffs similar to those reported here. Since in the experiments the calcium concentration is collected from a volume of 1.0 fl (1.0 μm^3), we averaged the calcium concentration over an area of 1.0 μm^2 with the cluster of IP_3Rs in the center. Each calcium release event that exceeded an amplitude of 20.0 nM was tracked and the maximum averaged Ca^{2+} concentration during the event was recorded as the amplitude. The cut-off concentration of 20.0 nM was chosen, as it lies between blip amplitudes (single-channel release events with amplitudes of ~30.0 nM) and noise background. Fig. 6 shows the amplitude distribution for various effective diffusion coefficients and IP_3 values. Fig. 6 *A* depicts the puff-amplitude distribution obtained experimentally by Thomas et al.(6). The overall agreement between the simulations and the experiments is best at an effective diffusion coefficient of $D = 30\ \mu m^2/s$, consistent with estimates for the effective diffusion coefficient obtained from confocal line-scan data (21). Fig. 6 *B* shows the puff-amplitude distribution obtained from our model for $D = 30\mu m^2/s$ and an IP_3 concentration of 5.5 μM. At those parameter values, the puffs have a mean amplitude of 215.0 nM and range between 50 and 600 nM, in excellent agreement with experimental data by Thomas et al. (6). As the diffusion coefficient D increases, the peak in the puff-amplitude distribution shifts toward smaller Ca^{2+} concentrations (Fig. 6 *C*), because the Ca^{2+} released through the IP_3Rs diffuses away more rapidly and the number of open channels during a single puff decreases.

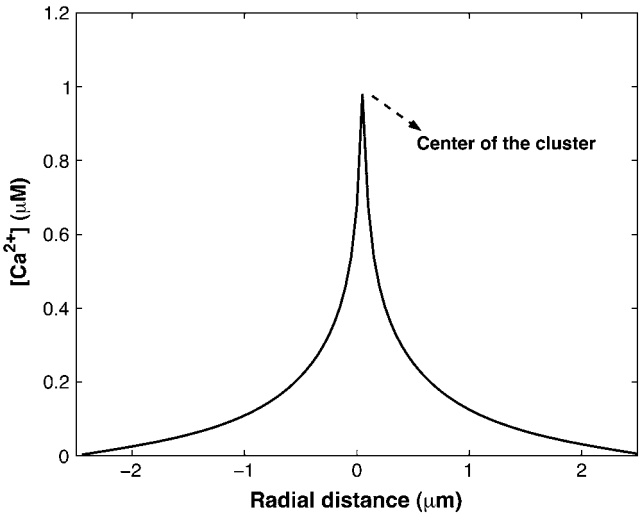

FIGURE 5 Spatial steady-state Ca^{2+} profile for a single open cluster in two spatial dimensions. Parameters different from those in Table 1 are: $D = 30.0\ \mu m^2\ s^{-1}$, $IP_3 = 5.0\ \mu$M, and $V_{cluster} = 600.0\ s^{-1}$.

The amplitude distribution and its peak also depends on the IP_3 concentration. Fig. 6, *B* and *D*, shows the puff-amplitude distributions for two concentrations of IP_3, 5.5 μM (*B*) and 10 μM (*D*). Although the peak of the distribution in *D* is at approximately the same calcium concentration as in *B*, it is more symmetric around the maximum in *D*. Furthermore, the average puff amplitude in *D* is larger. The latter occurs because at larger IP_3 concentrations the open probabiliity of an IP_3R is larger and hence more channels open during a release event, increasing the release of Ca^{2+}. This behavior is consistent with the experimental observation of Thomas et al. (6), where it has been shown that the peak of the puff-amplitude distribution shifts toward larger values as the histamine concentration (the agonist) increases (Fig. 5 of Thomas et al. (6)). The peak in Fig. 6 *B* resembles more the saw-toothed shape of the experimental puff-amplitude distribution. The amplitude distribution from our simulations is also qualitatively similar to the amplitude distribution of puffs from *Xenopus* oocytes (compare Fig. 6 with Fig. 8 *A* of Sun et al. (5)). Since the amplitude distribution obtained from HeLa cells in Thomas et al. (6) is calibrated in nanomolars (rather than fluorescence units), we use those amplitudes for quantitative comparison. Tovey et al. (2) showed that the kinetics of puffs are similar in various cells with different

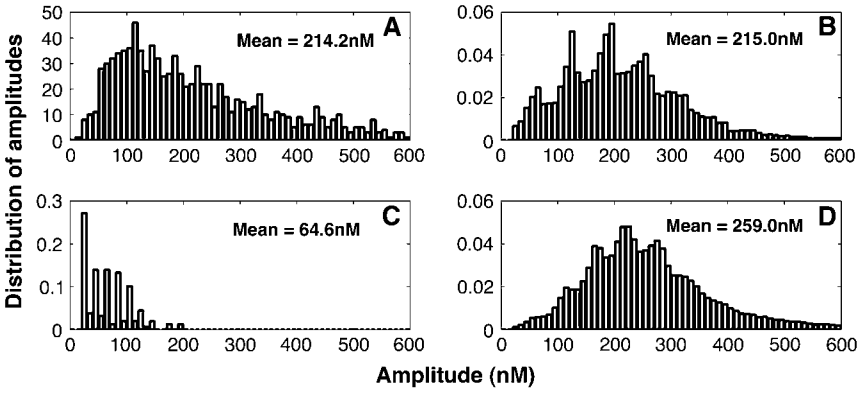

FIGURE 6 Amplitude distribution of puffs with various diffusion coefficients and IP_3 concentrations. (*A*) Experimental data. The vertical axis represents the number of events obtained for corresponding amplitudes. (*B*) $D = 30.0\ \mu m^2\ s^{-1}$. (*C*) $D = 100.0\ \mu m^2\ s^{-1}$. (*D*) $IP_3 = 10\ \mu M$, $D = 30\ \mu m^2\ s^{-1}$. (*B–D*) $V_{cluster} = 800.0\ s^{-1}$. The experimental data have been estimated by eye from Fig. 3 of Thomas et al. (6).

relative abundances of IP_3R isoforms. We therefore hope that the results from our simulations are comparable to puffs from various cell types.

Lifetime distribution of Ca^{2+} puffs

A detailed examination of the elementary calcium release events obtained with improved resolution not only revealed variability in puff amplitudes but also their time course. Despite being evoked by identical stimulus strengths, the durations of the puffs varied almost 10-fold (5–7). The lifetime of puffs, or the FDHM, is defined as the time during which the calcium concentration at the puff site remains above one-half of the maximal value. Fig. 7 shows lifetime distributions of puffs for various diffusion coefficients and IP_3 values. Experimental data by Sun et al. (5) are shown in Fig. 7 *A*. Fig. 7 *B* shows the distribution of lifetimes obtained from our model at $D = 30\ \mu m^2/s$ and an IP_3 concentration of 5.5 μM. Both distributions (Fig. 7, *A* and *B*) exhibit a rise, a subsequent maximum at ~100 ms and then a decay to zero at ~600 ms. At short times, however, the experimental distribution and the model predictions seem to be different. This discrepancy is likely to be caused by a cut-off in the experimental protocol (for a more detailed discussion, see the next section). The peak of the puff lifetime distribution shifts toward smaller lifetimes as the diffusion coefficient D increases (Fig. 7 *C*). This shift in the distribution occurs because for larger diffusion coefficients, calcium diffuses more rapidly away from the puff site, causing a decrease in the open probability for more channels and, hence, duration of puffs. Similar to the mean of the amplitude distribution, which shifts to larger amplitudes with increasing IP_3 concentration, the peak of the lifetime distribution shifts to larger lifetimes for increasing IP_3 concentration. In Fig. 7, *B* and *D*, we compare the puff lifetime distribution at $D = 30\ \mu m^2/s$ for IP_3 concentrations of 5.5 μM (*B*) and 10 μM (*D*).

Correlation of lifetime and amplitude of puffs

In the experiment, only a small correlation was observed between the lifetime and the amplitude of puffs (Fig. 3 *C b* of Thomas et al. (6)). To test our model for such behavior, we calculated the correlation between puff amplitude A and lifetime T using

$$C = \frac{\langle (A - \langle A \rangle)(T - \langle T \rangle) \rangle}{(\langle (A - \langle A \rangle)^2 \rangle)^{1/2} (\langle (T - \langle T \rangle)^2 \rangle)^{1/2}}, \tag{8}$$

where $\langle\ \rangle$ indicates temporal averaging.

We find that our simulations predict correlation values of $C \approx 0.31$ for various IP_3 concentrations and calcium diffusion coefficients (we tested for $4\ \mu M < IP_3 < 7\ \mu M$ and $20\ \mu m^2/s < D < 35\ \mu m^2/s$). It is therefore expected that the

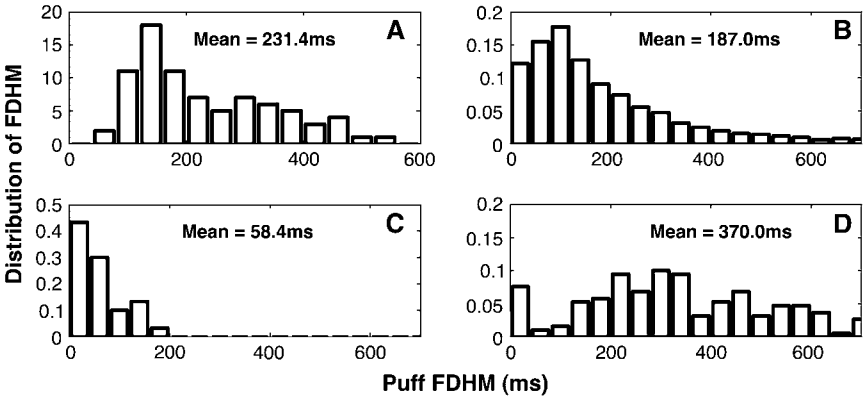

FIGURE 7 Distribution of puff widths at various values of the diffusion coefficient and IP_3 concentration. (*A*) Experimental data, estimated by eye from Fig. 2 of Sun et al. (5). The vertical axis represents the number of events for the corresponding duration. (*B*) $D = 30.0\ \mu m^2\ s^{-1}$. (*C*) $D = 100.0\ \mu m^2\ s^{-1}$. (*D*) $IP_3 = 10\ \mu M$, $D = 30\ \mu m^2\ s^{-1}$, and $V_{cluster} = 800\ s^{-1}$.

puffs with larger amplitudes will have larger lifetimes. However, this is not a strict rule and it is possible to observe puffs with smaller amplitude but larger lifetime and vice versa. Fig. 8 shows a scatter plot of puff amplitude versus lifetime at $IP_3 = 5.0\ \mu M$ and $D = 30.0\ \mu m^2\ s^{-1}$. Similar behavior can be seen for other IP_3 concentrations and values for D (results not shown here).

Interpuff-interval distribution of puffs

Another important characteristic of calcium puffs is the distribution of time intervals between two consecutive puffs. Marchant et al. (1) showed that a single puff cannot initiate a calcium wave by itself. However, several puffs at discrete sites coordinate to initiate a global response. The authors showed that the frequency of puffs increases before a wave is initiated. Also the interpuff interval becomes shorter (Figs. 8 and 10 of Marchant et al. (1)) before the generation of a wave. Their experimental investigation revealed interpuff-interval distributions that exhibit a single peak at ~1.5 s or 3.4 s, depending on whether the puffs are focal or nonfocal. The interpuff interval distribution obtained from our model is shown in Fig. 9 for various IP_3 concentrations and diffusion coefficients D. As shown in Fig. 9 *A*, the distribution shifts toward smaller times as the IP_3 concentration increases. For increasing diffusion coefficients, the distribution shifts toward larger times (Fig. 9 *B*). This increase occurs because the increased diffusion removes the calcium rapidly from the puff site, decreasing the chance for the channels to be reactivated.

Width distribution

The spatial spread of puffs can vary between events, depending on their amplitude and channel open-times during each event. Haak et al. (7) analzyed the spatial spread of Ca^{2+} sparks and puffs in oligodendrocyte progenitors. They showed that the phospholipase C/IP_3-linked muscarinic agonist MeCh-evoked puffs showed a spatial width distribution from ~0.5 to ~3.5 μm and peaked around 1.75 μm. In a separate set of experiments, Machacha (27) found puffs with an average width of ~2.0 μm in oocytes and a little wider in eggs.

Fig. 10 shows the distribution of spatial puff width obtained from our simulations at IP_3 concentrations of 5 μM (Fig. 10 *B*) and 6 μM (Fig. 10 *C*). To compute the spatial spread of puffs, we recorded the maximum calcium concentration at the cluster during each event at the center of the patch. The FWHM is defined as twice the radial distance from the center to the points where the Ca^{2+} concentration has decreased to half of the amplitude at the center. As shown in Fig. 10, the distribution shifts toward larger values as IP_3 increases.

The agreement between data (Fig. 10 *A*) and simulations (Fig. 10, *B* and *C*) is not very good, most likely since we did not explicitly take into account the buffer kinetics.

DISCUSSION

Elementary Ca^{2+} release events such as puffs and blips are at the basis of local Ca^{2+} signaling and can act as building blocks to generate global events like waves and oscillations (1–4). The characteristics of such elementary Ca^{2+} release events convey important information about the gating and spatial distribution of the intracellular Ca^{2+} release channels through which these events are generated. However, due to the limitations of microfluorimetric detection methods, neither the spatial dimensions nor the actual contents could

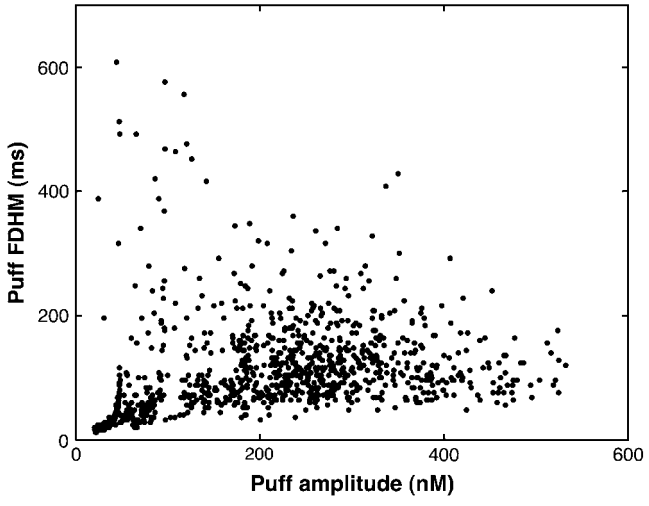

FIGURE 8 The scatter plot of puff FDHM versus puff amplitude demonstrates small correlations between lifetime and amplitude of puffs. Parameters not given in Table 1: $IP_3 = 5.0\ \mu M$, $V_{Cluster} = 600.0\ s^{-1}$, and $D = 30.0\ \mu m^2\ s^{-1}$.

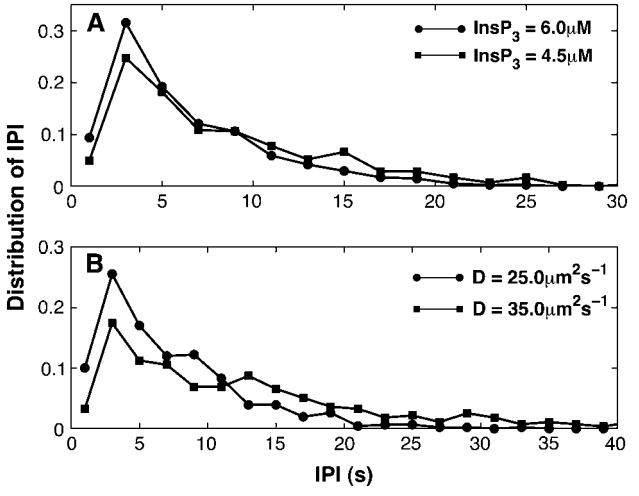

FIGURE 9 Interpuff interval distribution of puffs at various IP_3 concentrations (*A*) and various values for the diffusion coefficient D (*B*). (*A*) $D = 25.0\ \mu m^2\ s^{-1}$. (*B*) $IP_3 = 5.0\ \mu M$. $V_{cluster} = 600.0\ s^{-1}$ for both panels *A* and *B*.

be estimated precisely. Hence, theoretical tools are used to estimate these features. We present here a stochastic model based on the kinetic Sneyd-Dufur model (16) that consistently describes multiple statistical features of elementary Ca^{2+} release events with one set of parameters. Such a model can be used in the future as a basic building block to accurately predict more complex features, such as whole-cell signaling behavior.

The model combines a stochastic model for the IP_3 receptor that incorporates recent insights about the kinetics of the IP_3 receptor with solving a partial differential equation for the spread of Ca^{2+} in the cytosol. We ignored the spatial resolution of the cluster and hence considered the cluster as a point source. This point-source approximation has been tested by simulations that take into account the spatial structure of the cluster (simulations performed with 20.0-nm grid size; results not shown). Consistent with the conclusion made by Swillens et al. (11), we conclude that the point-source approximation is accurate. The parameters used here to mimic the statistical properties of blips and puffs are based on estimates in Sneyd et al. (16) for whole-cell Ca^{2+} signaling. Although the statistical properties of the elementary Ca^{2+} puffs critically depend on the values of these parameters, this set of parameters—without further adjustment—led to good overall agreement between experimentally observed features such as puff amplitude and lifetime distributions and model predictions. We ignored the complicating effects of Ca^{2+} buffers (19,20). To minimize these effects, we used the rapid buffering approximation of Wagner and Keizer (20) and the effective diffusion constant $D = \sim 30.0\ \mu m^2\ s^{-1}$, which is reduced in comparison to the diffusion coefficient of free Ca^{2+} to account for Ca^{2+}-binding to buffers (28). Our numerical simulations confirm that puffs and blips vary in amplitude, duration, spatial spread, and interpuff interval (Figs. 4–10). The variation in these characteristics is due to the variability in the number of channels recruited and the open time of channels during individual puffs. Thus, our results indicate that a fixed puff morphology, which has been used previously (29), is not a good assumption for analysis of elementary Ca^{2+} release events.

Using the approach discussed in the Materials and Methods, we were able to generate numerous features of the experimentally observed statistical properties of calcium puffs. Consistent with the theoretical study of Swillens et al. (11), our model predicts single-peak amplitude distributions for various IP_3 concentrations that have been consistently observed in experiments (5–7). An improvement over the results from Swillens et al. (11) occurred in that the shape of the distributions and range of amplitude values are quantitatively close to those observed by Parker's group (5) and Bootman's group (6). Although the amplitude distribution predicted by the model in Swillens et al. (11) has a peak that is close to the experimental value, the range of the amplitudes is much smaller than that observed experimentally (see Fig. 4, *A* and *B*, of Swillens et al. (11)). By increasing the IP_3 concentration in (11) arbitrarily, the range of amplitudes can be shifted to the experimentally observed values, but the maximum of the distribution moves to a too-large value.

Determining the shape and range of puff lifetime distributions was the primary motivation of this study. In experiments, a distribution with a single peak and a subsequent exponential decay has been found. Parker and coworkers showed that lifetime distributions of puffs span a range of values from 15 to 600 ms, with a peak at ~150 ms (5). Thomas et al. (6) reported a similar distribution. The theoretical study of Shuai et al. (10), using a stochastic version of the Li-Rinzel model (15), led to a single-peak distribution, but the predicted lifetimes are about one order of magnitude too large. As shown in Fig. 4, *D* and *F*, the puffs obtained from the more detailed stochastic De Young-Keizer model (14) are also much wider in temporal extent than those observed experimentally. The main reason for the prolonged puffs predicted with the De Young-Keizer model is the rapid binding and unbinding of IP_3 that leads to rapid sequences of channel opening and thus long cumulative opening before the subunit inactivates. We were not able to correct this feature of the De Young-Keizer model by adjusting parameters, since the required dramatic changes would strongly interfere with other desired features such as those present in the generation of Ca^{2+} oscillations. In the Sneyd-Dufour model, these rapid bindings and unbindings do not occur. The subunit rapidly inactivates after it is activated, thus producing short channel open times.

Our model predicts a lifetime distribution (Fig. 7) that is in good overall agreement with the experimental findings of Sun et al. (5). However, our model predicts more events with shorter durations compared to that observed in the experiment (note the larger bars at FDHM ≈ 50 ms in Fig. 7). This difference could be caused by the experimental protocol used

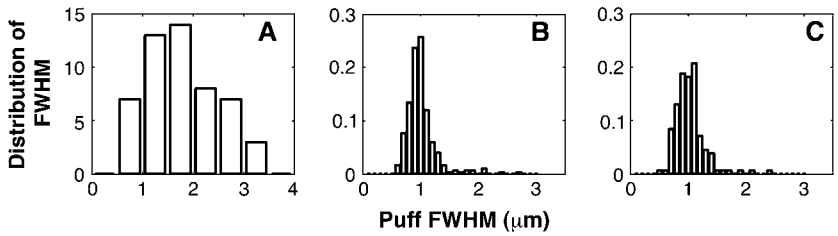

FIGURE 10 Distribution of spatial widths of Ca^{2+} puffs at various values of the IP_3 concentration. (*A*) Experimental data obtained from Haak et al. (7). The vertical axis represents the number of events obtained with the corresponding width. (*B*) $IP_3 = 5.0\ \mu M$. (*C*) $IP_3 = 6.0\ \mu M$. Parameters not given in Table 1: $V_{Cluster} = 600.0\ s^{-1}$; $D = 25.0\ \mu m^2\ s^{-1}$.

by Parker et al. (30). They argued that the approximately Gaussian distribution of ''blips'' (Fig. 3 *B* of Parker and Yao (30)) might be based on the fact that many undetectable ''blips'' had been ignored. Motivated by this comment, we increased the cut-off level for puffs to 40.0 nm and indeed obtained a distribution that resembles that found in the experiment for short puffs as well (results not shown).

The variations in amplitude and duration of puffs are related to the variations in number and duration of open IP_3Rs in the cluster. Often, a large number of open channels corresponds to puffs of large amplitude and long duration (Fig. 4, *A* and *C*). However, a large puff may also be caused by a small fraction of open IP_3Rs, but with long open times. Our model typically predicts 4 to 10 open channels during a puff (see Fig. 4 *C*), which is consistent with other studies and experimental data (5,10,11).

Consistent with the experimental findings, our stochastic model predicts a single-peak distribution of interpuff intervals. The model further predicts a shift of the distribution toward smaller values as the IP_3 concentration is increased. Marchant et al. (1) showed that the distribution of interpuff intervals peaks around time intervals of 1.5 s and 3.4 s, depending on whether the puffs are focal or nonfocal. The interpuff interval distributions for focal puffs peaks at a smaller interval value than those of nonfocal puffs. They also showed that global calcium waves can be initiated only with a larger IP_3 stimulus. Thus, it is expected that the interpuff interval distribution will shift toward smaller intervals, or, equivalently, the frequency of puffs will increase as the IP_3 concentration is increased (see Marchant et al. (1) for details). A similar behavior is observed in our model, where the mean interval shifts toward shorter intervals as the IP_3 concentration is increased (Fig. 9 *A*).

The diffusion coefficient also has an effect on interpuff interval distribution (Fig. 9 *B*). The distribution shifts slightly to larger intervals when the diffusion coefficient is increased. However, on the larger scale, that does not necessarily indicate that increased diffusion reduces the chance for puffs to initiate global calcium waves. Increased diffusion can coordinate the neighboring puff sites more effectively and thus cause a global calcium response.

The study presented here has important implications for modeling of intracellular calcium signaling and downstream processes. Calcium release from stores can signal different messages, depending on the spatial extent, amplitude, and frequency of the calcium elevation (for a recent review, see Niggli (31)), depending on the system that decodes the calcium signals. The time course of the puffs is important for, e.g., nuclear functions such as transcription (32), since local cytosolic increases of Ca^{2+} cause increases in nuclear Ca^{2+}, which in turn regulate transcription. Hence, it is important that a model for local calcium elevation describes the amplitudes, durations, and frequencies quantitatively correctly. We present here a model that accurately describes all these features with one set of parameters.

APPENDIX

The purpose of this appendix is to show that the assumption that all IP_3 channels are exposed to the same Ca^{2+} concentration within one cluster is justified, although the point-souce approximation yields a profile that seems to indicate otherwise. To this end, we consider a simplified one-dimensional system with a cluster of length $2a$. The source of Ca^{2+} is evenly distributed over the interval $[-a, a]$ of the x axis. Ca^{2+} released into the one-dimensional space diffuses and is absorbed with a linear rate γc. The diffusion equation is given by

$$\frac{\partial c}{\partial t} = D\frac{\partial^2 c}{\partial x^2} - \gamma c + \tilde{j}\,\mathrm{rect}(x, x_0), \tag{9}$$

where $\tilde{j}$ describes the source density of Ca^{2+} (concentration c) and $\mathrm{rect}(x, a) = 1$ for $|x| < a$ and $\mathrm{rect}(x, a) = 0$ otherwise. The steady-state profile is given by the solution of the ordinary differential equation

$$\frac{\partial^2 c}{\partial x^2} = \kappa^2 c - \frac{\tilde{j}}{D}\,\mathrm{rect}(x, a), \tag{10}$$

where $\kappa^2 = \gamma/D$. Solving Eq. 10 for $|x| < a$ and $|x| > a$ separately, with the integration constants obtained by requiring a profile that is continuous and once differentiable at $x = \pm a/2$ (which is a feature that follows directly from Eq. 10 by integrating over an ε-interval around $x = \pm\, a/2$) we find the solution in dimensionless variables $\bar{x} = \kappa x, \bar{a} = \kappa a$

$$c(\bar{x}) = \begin{cases} \dfrac{j}{2D\kappa}\dfrac{1}{\bar{a}}\dfrac{\sinh(\bar{a})}{\cosh(\bar{a}) + \sinh(\bar{a})}\exp(-(|\bar{x}| - \bar{a})) & \text{for} |\bar{x}| > \bar{a} \\ \dfrac{\tilde{j}}{2D\kappa}\dfrac{1}{\bar{a}}\left(1 - \dfrac{\cosh(\bar{a})}{\cosh(\bar{a}) + \sinh(\bar{a})}\right) & \text{for} |\mathrm{x}| < \bar{a} \end{cases}, \tag{11}$$

with $j \equiv 2a\tilde{j}$.

Using the point-source approximation, we replaced the distributed source by a point source with the same total flux $j = 2a\tilde{j}$ as the distributed source, i.e.

$$\frac{\partial c}{\partial t} = D\frac{\partial^2 c}{\partial x^2} - \gamma c + j\delta(x). \tag{12}$$

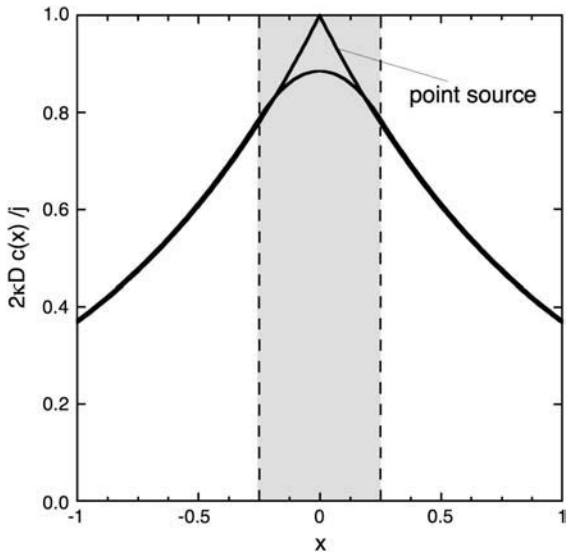

FIGURE 11 The one-dimensional steady-state profiles obtained in Eqs. 11 and 14 are compared. The shaded interval represents the spatial extent of the cluster. The point-exact solution is relatively flat inside the cluster, whereas the point-source solution exhibits a sharp peak at the point source.

The steady-state profile is determined by the ordinary differential equation

$$\frac{\partial^2 c}{\partial x^2} = \kappa^2 c - \frac{j}{D}\delta(x), \tag{13}$$

with $\delta(x)$ the Dirac's δ function. Solving this equation for $x < 0$ and $x > 0$ separately, and matching the solution such that the profile is continuous and the first derivative has a discontinuity $c'(0_+) - c'(0_-) = -j/D$ (obtained by integrating Eq. 13 from $-\varepsilon$ to ε), one finds the solution in dimensionless units $\bar{x} = x\kappa$,

$$c(\bar{x}) = \frac{j}{2\kappa D} e^{-|\bar{x}|}. \tag{14}$$

It is straightforward to see that both solutions (11,14) are identical in the limit $a \to 0$. For $\bar{a} = 0.25$, i.e., when the diffusion-length $1/\kappa$ is twice the cluster size, we compare both solutions in Fig. 11. It is clear that outside the cluster $|x| > a$, both solutions agree well, whereas inside the cluster the actual profile is relatively flat, justifying the assumption that all IP_3Rs are clamped to the same Ca^{2+} concentration. The sharp profile in Fig. 5 is thus an artifact of the point-source approximation within the spatial extent of the cluster and does not indicate that the Ca^{2+} concentration varies dramatically within the cluster.

This material is based upon work supported by the National Science Foundation (IOB-0345500).

REFERENCES

1. Marchant, J., N. Callamaras, and I. Parker. 1999. Initiation of IP_3-mediated Ca^{2+} waves in *Xenopus* oocytes. *EMBO J.* 18:5285–5299.
2. Tovey, C. S., D. P. Smet, P. Lipp, D. Thomas, K. W. Young, L. Missiaen, D. H. Smedt, J. B. Parys, M. J. Berridge, J. Thuring, A. Holmes, and M. D. Bootman. 2001. Calcium puffs are generic IP_3-activated elementary calcium signals and are downregulated by prolonged hormonal stimulation to inhibit cellular calcium responses. *J. Cell Sci.* 114:3979–3989.
3. Callamaras, N., J. S. Marchant, X. P. Sun, and I. Parker. 1998. Activation and coordination of IP_3-mediated elementary Ca^{2+} events during global Ca^{2+} signals in *Xenopus* oocytes. *J. Physiol.* 509:81–91.
4. Bootman, M., E. Niggli, M. Berridge, and P. Lipp. 1997. Imaging the hierarchical Ca^{2+} signalling system in HeLa cells. *J. Physiol.* 499: 307–314.
5. Sun, X. P., N. Callamaras, J. S. Marchant, and I. Parker. 1998. A continuum of IP_3-mediated elementary Ca^{2+} signalling events in *Xenopus* oocytes. *J. Physiol.* 509:67–80.
6. Thomas, D., P. Lipp, M. J. Berridge, and M. D. Bootman. 1998. Hormone-evoked elementary Ca^{2+} signals are not stereotypic, but reflect activation of different size channel clusters and variable recruitment of channels within a cluster. *J. Biol. Chem.* 273:27130–27136.
7. Haak, L. L., L. S. Song, T. F. Molinski, I. N. Pessah, H. Cheng, and J. T. Russell. 2001. Sparks and puffs in oligodendrocyte progenitors: cross talk between ryanodine receptors and inositol trisphosphate receptors. *J. Neurosci.* 21:3860–3870.
8. Falcke, M. 2004. Reading the patterns in living cells—the physics of Ca^{2+} signaling. *Adv. Phys.* 53:255–440.
9. Falcke, M., L. Tsimring, and H. Levine. 2000. Stochastic spreading of intracellular Ca^{2+} release. *Phys. Rev. E.* 62:2636–2643.
10. Shuai, J. W., and P. Jung. 2002. Stochastic properties of Ca^{2+} release of inositol 1,4,5-trisphosphate receptor clusters. *Biophys. J.* 83: 87–97.
11. Swillens, S., G. Dupont, L. Combettes, and P. Champeil. 1999. From calcium blips to calcium puffs: theoretical analysis of the requirements for interchannel communication. *Proc. Natl. Acad. Sci. USA.* 96: 13750–13755.
12. Taylor, W. C., P. C. A. da Fonseca, and E. P. Morris. 2004. IP_3 receptors: the search for structure. *Trends Biochem. Sci.* 29:210–219.
13. Shuai, J. W., and P. Jung. 2003. Optimal ion channel clustering for intracellular calcium signaling. *Proc. Natl. Acad. Sci. USA.* 100:506–510.
14. DeYoung, G. W., and J. Keizer. 1992. A single pool inositol 1,4,5-trisphosphate-receptor-based model for agonist stimulated oscillations in Ca^{2+} concentration. *Proc. Natl. Acad. Sci. USA.* 89:9859–9899.
15. Li, Y. X., and J. Rinzel. 1994. Equations for InsP3 receptor-mediated Ca^{2+} oscillations derived from a detailed kinetic-model: a Hodgkin-Huxley like formalism. *J. Theor. Biol.* 166:461–473.
16. Sneyd, J., and J. F. Dufour. 2002. A dynamic model of the type-2 inositol trisphosphate receptor. *Proc. Natl. Acad. Sci. USA.* 99:2398–2403.
17. Sneyd, J., K. Tsaneva-Atanasova, D. I. Yule, J. L. Thompson, and T. J. Shuttleworth. 2004. Control of calcium oscillations by membrane fluxes. *Proc. Natl. Acad. Sci. USA.* 101:1392–1396.
18. Dargan, L. S., and I. Parker. 2003. Buffer kinetics shape the spatiotemporal patterns of IP_3-evoked Ca^{2+} signals. *J. Physiol.* 553:775–788.
19. Falcke, M. 2003. Buffers and oscillations in intracellular Ca^{2+} dynamics. *Biophys. J.* 84:28–41.
20. Wagner, J., and J. Keizer. 1994. Effects of rapid buffers on Ca^{2+} diffusion and Ca^{2+} oscillations. *Biophys. J.* 67:447–456.
21. Yao, Y., J. Choi, and I. Parker. 1995. Quantal puffs of intracellular Ca^{2+} evoked by inositol trisphosphate in *Xenopus* oocytes. *J. Physiol.* 482:533–553.
22. Swillens, S., P. Champeil, L. Combettes, and G. Dupont. 1998. Stochastic simulation of a single inositol 1,4,5-trisphosphate-sensitive Ca^{2+} channel reveals repetitive opening during 'blip-like' Ca^{2+} transients. *Cell Calcium.* 23:291–302.
23. Gillespie, D. 1976. General method for numerically simulating stochastic time evolution of coupled chemical reactions. *J. Comput. Phys.* 22:403–434.
24. Burden, L. R., and J. D. Faires. 2001. Numerical Analysis, 7th Ed. Brooks/Cole, Stamford, CT.
25. Bird, J. G., K. G. Oliver, D. A. Horstman, J. Obie, and W. Putney, Jr. 1991. Relationship between the calcium-mobilizing action of inositol 1,4,5-trisphosphate in permeable AR4–2J cells and the estimated levels of inositol 1,4,5-trisphosphate in intact AR4–2J cells. *Biochem. J.* 273: 541–546.
26. Leybaert, L., K. Paemeleire, A. Strahonja, and M. J. Sanderson. 1998. Inositol-trisphosphate-dependent intercellular calcium signaling in and between astrocytes and endothelial cells. *Glia.* 24:398–407.
27. Machaca, K. 2004. Increased sensitivity and clustering of elementary Ca^{2+} release events during oocyte maturation. *Dev. Biol.* 275:170–182.
28. Keizer, J., G. D. Smith, S. Ponce-Dawson, and J. E. Pearson. 1998. Saltatory propagation of Ca^{2+} waves by Ca^{2+} sparks. *Biophys. J.* 75: 595–600.
29. Huser, J., and L. A. Blatter. 1997. Elementary events of agonist-induced Ca^{2+} release in vascular endothelial cells. *Am. J. Physiol.* 273: C1775–C1782.
30. Parker, I., and Y. Yao. 1996. Ca^{2+} transients associated with openings of inositol trisphosphate-gated channels in *Xenopus* oocytes. *J. Physiol. (Lond.).* 491:663–668.
31. Niggli, E. 1999. Localized intracellular calcium signaling in muscle: calcium sparks and calcium quarks. *Annu. Rev. Physiol.* 61:311–335.
32. Lipp, P., D. Thomas, M. J. Berridge, and M. D. Bootman. 1997. Nuclear calcium signalling by individual cytoplasmic calcium puffs. *EMBO J.* 16:7166–7173.